INTERNATIONAL JOURNAL FOR NUMERICAL METHODS IN FLUIDS
Int. J. Numer. Meth. Fluids 2008; **57**:839–859
Published online 6 November 2007 in Wiley InterScience (www.interscience.wiley.com). DOI: 10.1002/fld.1648

Numerical investigation of the effects of sluice spillway roof profiles on the hydraulic characteristics

M. R. Bhajantri[1,2], T. I. Eldho[1,*,†] and P. B. Deolalikar[2]

[1]*Department of Civil Engineering, Indian Institute of Technology, Powai, Mumbai 400 076, India*
[2]*Central Water & Power Research Station, Khadakwasla, Pune, India*

SUMMARY

There is a need for evolving hydraulically efficient roof profile of bellmouth for high head sluice spillways, as sluice roof is susceptible to cavitation damage. In this paper, formulation and development of a numerical model for simulating the spillway flow and its application to a sluice spillway are presented. The main focus of the simulation study is to apply the developed model to investigate the effects of sluice roof profile geometry on the pressure distribution, the discharge coefficient and the nature of flow regime within the sluice bellmouth. From the analysis of results for eight different roof profiles by varying the entry and exit angles of elliptic bellmouth transition, some important observations have been suggested, which are of practical relevance to hydraulic design engineers. The numerical model results are compared for one profile with physical model study. The simulated results are in close agreement with the measured values. Copyright © 2007 John Wiley & Sons, Ltd.

Received 19 February 2007; Revised 8 September 2007; Accepted 25 September 2007

KEY WORDS: sluice spillway; roof profile; weakly compressible flow; finite volume method; pressure distribution; cavitation

1. INTRODUCTION

Dam building activities over the years have been concentrated in the ideal and easy sites, sparing the geologically and topographically complex and difficult sites for future activities. Attention is now focused on developing run-of-the-river hydroelectric projects in high mountains with narrow and elongated river basins with steep gradients, which are suitable for flushing. Innovative design of spillway such as sluice spillway is being implemented currently, which can handle both flood disposal as well as sediment flushing. Sluice spillway, a large capacity outlet placed in the body of the dam, fulfills both the objectives of surplussing the floodwater and flushing of sediment

*Correspondence to: T. I. Eldho, Department of Civil Engineering, Indian Institute of Technology, Mumbai 400 076, India.
†E-mail: eldho@civil.iitb.ac.in

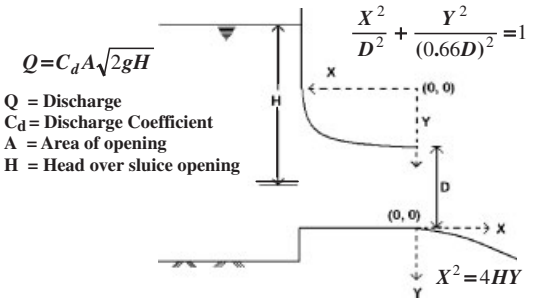

Figure 1. Definition sketch of sluice spillway.

through the spillway. Sluice spillway would allow the setting of its crest at significantly lower elevation, yet retaining the choice of a high dam for creating head for power generation. The parameters affecting the performance of sluice spillway are: head over the opening, size of the sluice barrel, entrance shape of the sluice bellmouth, thickness of intermediate piers and approach flow conditions. Figure 1 shows the definition sketch of sluice spillway. The water from the reservoir approaching the sluice bellmouth opening should be accelerated smoothly to minimize contraction losses and to avoid low pressures resulting in cavitation damages. If the entrance curve is too sharp or too short, flow instabilities may induce sub-atmospheric pressures. Normally, an elliptical transition curve recommended by United States Bureau of Reclamation (USBR) is adopted defined by the equations [1]:

$$\frac{X^2}{D^2}+\frac{Y^2}{(0.33D)^2}=1 \tag{1a}$$

$$\frac{X^2}{D^2}+\frac{Y^2}{(0.66D)^2}=1 \tag{1b}$$

where D is the vertical height of the sluice opening. If reservoir bed upstream of spillway is very close to the sill level of the sluice, the profile defined by Equation (1b) is used. It has been experienced from the physical model studies that the flow through sluice barrel do not get fully developed and that flow separation takes place on the sluice roof profile, resulting in negative pressure for high head spillways. Such high head sluice spillways should be checked against presence of sub-atmospheric pressures on the bellmouth roof to avoid cavitation damages.

A common solution to this is by way of constricting the sluice cross section at the end to induce pressurized flow in the sluice barrel. However, a proper solution will be to evolve a suitable roof profile that would ensure adhering of flow closely to the roof profile to have acceptable pressure distribution. A literature survey revealed that such studies have not been done either on the physical model or on the numerical model. The present numerical study, therefore, attempts to investigate the influence of sluice roof shape on the pressure distribution and other flow features.

Spillway flows are investigated through physical or numerical modeling. The drawbacks associated with physical model studies of spillways are cost of construction, delay in time for fabrication and construction of model parts and conducting experiments and the difficulty in changing structural details of various components of spillway while doing parametric studies. Numerical simulation has become a viable complementary tool to physical modeling of spillway flows. The data obtained

DOI: 10.1002/fld

from the physical model studies can be used for model calibration and validation of the numerical models. The advantages of both physical and numerical models should be exploited judiciously to optimize the spillway design.

Most of the researchers have used either potential flow theory [2] or Reynolds-averaged Navier–Stokes (RANS) equations [3–6] and available commercial codes [7–9]. Unami *et al*. [10] developed depth-averaged 2-D numerical model of spillway flow using both finite element method (FEM) and finite volume method (FVM). Space-averaged Navier–Stokes equations had been used by Zhou and Bhajantri [11], Song and Zhou [12] to develop 2-D and 3-D models, respectively. FVM and FEM are more suitable for modeling spillways flows for their suitability to deal with complicated boundaries. While most of the literature available on numerical modeling of spillway flows deals with more conventional ogee spillway, the present paper deals with numerical modeling of submerged type or sluice spillway.

In this study, for the analysis of sluice spillway, a 2-D vertical model is used, which is based on weakly compressible flow theory [13]. Typical flows over spillway are of large Reynolds number type and are characterized by hydrodynamic pressure distribution. These flows are of small Mach number ($M<0.3$) and usually regarded as weakly compressible flows. The weakly compressible flow equations are applicable and efficient for all practical flows of small Mach number and large Reynolds number such as flow over spillway. Both physically and computationally, the water is not quite the same as the ideal fluid flow. Hence, it is legitimate to use the compressible form of equations even for the so-called incompressible flows. Compressibility is incorporated in order to make the problem more amenable to numerical solution of incompressible flows. The artificial compressibility formulation for hydrodynamic flow calculations is getting popularity for its simplicity and efficiency. Another alternative method of introducing compressibility term is by modifying the compressible form of continuity equation for low Mach number flows. The compressibility term in this approach is not artificial. The present paper describes a 2-D model to investigate the flow over spillway. This model, which is based on body fitted explicit FVM, has been used for the analysis of broad crested spillway and the sluice spillway [14, 15]. In the present study, the influence of various roof profiles on pressure and other flow characteristics are investigated for sluice spillway. The second-order predictor–corrector scheme was used to solve the equations [16].

2. NUMERICAL MODELING OF SPILLWAY FLOW

2.1. Governing equations

The equation of continuity for compressible hydrodynamic flow (weakly compressible flow) can be expressed as follows [13]:

$$\frac{\partial p}{\partial t}+\rho_0 a_0^2 \nabla\cdot\mathbf{V}=0 \tag{2}$$

and the equation of motion can be expressed as

$$\frac{\partial \mathbf{V}}{\partial t}+\mathbf{V}\cdot\nabla\mathbf{V}+\frac{1}{\rho_0}\nabla p=0 \tag{3}$$

where p is the pressure, ρ the density of the fluid, a the speed of the sound and V the velocity.

DOI: 10.1002/fld

The subscript 0 represents the reference condition. The flow that satisfies Equations (2) and (3) is called Euler form of a weakly compressible flow.

The authenticity of using the Euler equations for simulation of spillway flows is based on the intuition that the interaction between the boundary layer and the inviscid portion of the flow field is negligible if the boundary is very thin compared with the characteristic length of the flow field. Spillway surface being very smooth, the shear stress at the solid boundary of spillway is negligible. This fact clarifies why researchers in the past used potential flow theory to analyze the spillway flows.

2.2. *Upstream and downstream boundary conditions*

The upstream boundary can be set up on a reservoir section at which the reservoir water level and the incoming discharge can be known. This section is chosen far away from the spillway crest to avoid the reflection effect. The boundary condition based on velocity distribution is

$$u = u_0(x_0, y) \tag{4}$$

$$v = 0, \quad \frac{\partial p}{\partial x} = 0 \tag{5}$$

where u and v are the velocity components in the x and y directions and u_0 is the velocity component in the x direction at the upstream boundary. The downstream open boundary can be chosen on a sloping section of the spillway where the flow is fully developed so that zero gradients of velocity and pressure can be assumed.

2.3. *Solid boundary condition*

The solid boundary conditions are achieved by defining the flow variables at the center of the phantom cells located on the other side of the solid boundary. Three kinds of solid boundary conditions (full slip, no slip and partial slip) are available. Full slip means tangential velocity at the inner grid is equal to the tangential velocity on the solid surface, while no slip means tangential velocity on the solid surface is zero; for partial slip condition, a wall function should be used. Solid boundary conditions are achieved for the numerical solution by defining the flow variables at the center of the phantom (imaginary) cells located on the other side of the solid boundary as shown in Figure 2. The velocity and pressure at the boundary surface depend on the respective values defined at the phantom cell. For the solid boundary condition, the velocity vector at the phantom cell has a normal component equal and opposite to that of the boundary cell. This ensures no fluid flow across the solid boundary. The concept of phantom cell at the solid boundary is depicted in Figure 2 while applying full slip. In the present study, full slip condition was used for velocity at the solid boundary of the spillway.

In addition to the velocity vectors, pressure has to be defined at the solid boundary. This is achieved by defining pressure values at the phantom cells. To consider the effect of centrifugal force due to a curved wall boundary, the pressure equation for the boundary face with radius of curvature R and unit outward normal n is given by

$$\frac{\partial p}{\partial n} = \pm\rho\frac{U_b^2}{R} \tag{6}$$

DOI: 10.1002/fld

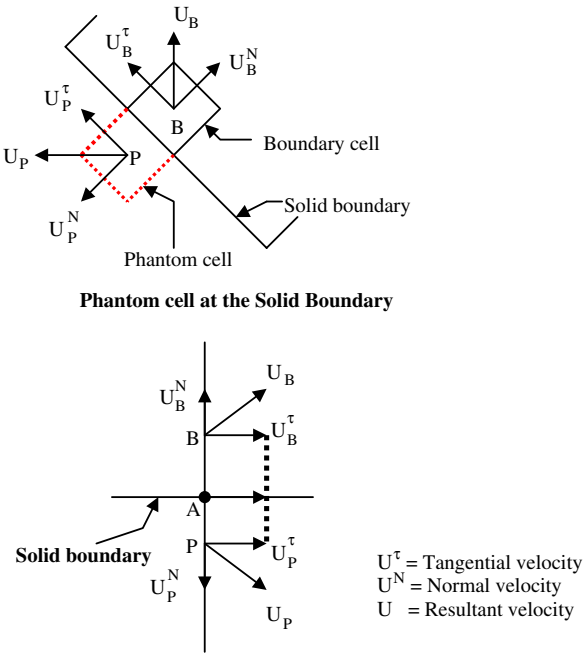

Figure 2. Full slip boundary condition on solid wall boundary.

where radius R of the solid surface can be calculated by the following formula:

$$R = \frac{[1+(\mathrm{d}y/\mathrm{d}x)^2]^{3/2}}{(\mathrm{d}^2y/\mathrm{d}x^2)} \tag{7}$$

where $y = f(x)$ is the equation of the solid boundary and U_b is the tangential velocity at the boundary cell. If the boundary face is straight, then the pressure at the phantom cell is considered same as that of the boundary cell.

2.4. *Free-surface boundary condition*

Free surface is simulated using kinematic and dynamic conditions. The kinematic condition is based on the idea that free surface is a material surface and has the form

$$\frac{\partial Z_\mathrm{f}}{\partial t} + \mathbf{u}\cdot\nabla Z_\mathrm{f} = v_\mathrm{f} \tag{8}$$

where Z_f is the free-surface displacement along the normal direction and; v_f is the free-surface velocity in the vertical direction. The dynamic boundary condition, ignoring the surface tension effect, is the zero stress condition. For this model, the dynamic boundary condition, which is zero stress on the free surface, is simplified as follows:

$$p = \text{atmospheric pressure}, \quad \frac{\partial \mathbf{V}}{\partial \mathbf{n}} = 0 \tag{9}$$

where $\mathbf{n}$ represents the unit vector normal to the free surface.

DOI: 10.1002/fld

2.5. Mesh generation

The supercritical flow is very sensitive to the geometric boundary condition. The smooth fitting of the boundary profile is essential to prevent a false wave generated by inaccurate representation of the boundary. A boundary fitted mesh system based on Thompson *et al.*'s method [17] is used in this study. The first step of Thompson's transformation is to specify the coordinates of the boundary grid. According to Thompson *et al.*'s theory, the original (x, y) domain is mapped onto a rectangular domain (ξ, η) by solving the following Poisson equations:

$$\xi_{xx} + \xi_{yy} = P(\xi, \eta) \tag{10a}$$

$$\eta_{xx} + \eta_{yy} = Q(\xi, \eta) \tag{10b}$$

where, x–y is the physical plane and ξ, η is the transformed plane. Equations (10a) and (10b) can be transformed to

$$\alpha x_{\xi\xi} - 2\beta x_{\xi\eta} + \gamma x_{\eta\eta} = -J^2[x_\xi P(\xi, \eta) + x_\eta Q(\xi, \eta)] \tag{11a}$$

$$\alpha y_{\xi\xi} - 2\beta y_{\xi\eta} + \gamma y_{\eta\eta} = -J^2[y_\xi P(\xi, \eta) + y_\eta Q(\xi, \eta)] \tag{11b}$$

where

$$\alpha = x_\eta^2 + y_\eta^2, \quad \beta = x_\xi x_\eta + y_\xi y_\eta, \quad \gamma = x_\xi^2 + y_\xi^2 \quad \text{and} \quad J = \frac{1}{(x_\xi y_\eta - y_\xi x_\eta)}$$

P and Q are the control functions used to adjust the distribution of grids [17].

The set of Equations (11a) and (11b) is solved iteratively by linearizing them. Suitable relaxation parameter (ω) is used for acceleration of convergence. A Von Neumann stability analysis of the linearized difference equations yields $0 \leqslant \omega \leqslant 2$ in order to guarantee stability of the numerical procedure.

Finite difference equations for the governing transformed equations are derived by approximating all derivatives with second order, central space difference. The resulting equations for X and Y at a point (i, j) in the computational plane are

$$\begin{aligned}
\overline{X}_{i,j} &= [\alpha(X^k_{i+1,j} + X^{k+1}_{i-1,j})/\Delta\xi^2 - 2\beta X_{\xi\eta} + \gamma(X^k_{i,j+1} \\
&\quad + X^{k+1}_{i,j+1})/\Delta\eta^2 + J^2(X_\xi P_{i,j} + X_\eta Q_{i,j})]/[2(\alpha/\Delta\xi^2 + \gamma/\Delta\eta^2)] \\
\overline{Y}_{i,j} &= [\alpha(Y^k_{i+1,j} + Y^{k+1}_{i-1,j})/\Delta\xi^2 - 2\beta Y_{\xi\eta} + \gamma(Y^k_{i,j+1} \\
&\quad + Y^{k+1}_{i,j+1})/\Delta\eta^2 + J^2(Y_\xi P_{i,j} + Y_\eta Q_{i,j})]/[2(\alpha/\Delta\xi^2 + \gamma/\Delta\eta^2)]
\end{aligned} \tag{12}$$

where $\Delta\xi$ and $\Delta\eta$ are the specified uniform sizes of the computational mesh and superscripts indicate the iteration number.

Since at all steps during the solution, the values for X and Y along the boundaries are known, Equation (12) constitutes a system of $(\text{imax}-2) \times (\text{jmax}-2)$ simultaneous nonlinear equations. This system of equations is solved iteratively using the point successive iteration method (SOR)

DOI: 10.1002/fld

as follows:

$$\begin{aligned} X_{i,j}^{k+1} &= \omega \overline{X}_{i,j} + (1-\omega) X_{i,j}^{k} \\ Y_{i,j}^{k+1} &= \omega \overline{Y}_{i,j} + (1-\omega) Y_{i,j}^{k} \end{aligned} \tag{13}$$

where superscripts denote the iteration number and ω is the acceleration parameter. Convergence of SOR at all interior points is guaranteed by requiring

$$\text{Max } (\delta S_{i,j}^2 / \delta S_{1i,j}^2), (\delta S_{i,j}^2 / \delta S_{2i,j}^2) \leqslant \varepsilon^2 \tag{14}$$

where ε is a pre-assigned small quantity (a typical value used for ε is 0.0001).

$$\delta S_{i,j}^2 = (X_{i,j}^{k+1} - X_{i,j}^{k})^2 + (Y_{i,j}^{k+1} - Y_{i,j}^{k})^2$$

$$\delta S_{1i,j}^2 = (X_{i+1,j}^{k} - X_{i,j}^{k})^2 + (Y_{i+1,j}^{k} - Y_{i,j}^{k})^2$$

$$S_{2i,j}^2 = (X_{i,j+1}^{k} - X_{i,j}^{k})^2 + (Y_{i,j+1}^{k} - Y_{i,j}^{k})^2$$

3. NUMERICAL SOLUTION

The governing differential equations are expressed in a conservative form and are integrated over control volumes defined by the mesh system [14, 15]. An explicit FVM is used to discretize the governing equations. The governing equations (2) and (3) are rewritten in a conservative form to apply an FVM scheme as follows:

$$\frac{\partial G}{\partial t} + \nabla \cdot \mathbf{F} = 0 \tag{15}$$

where G is the flow variable (p, u, v) and F is the flux vector. Equation (15) can be expressed in matrix form as follows:

$$\frac{\partial}{\partial t} \begin{bmatrix} p \\ u \\ v \end{bmatrix} + \nabla \cdot \begin{bmatrix} ku & kv \\ u^2 + \dfrac{p}{\rho_0} & uv \\ uv & v^2 + \dfrac{p}{\rho_0} \end{bmatrix} = \begin{bmatrix} 0 \\ 0 \\ 0 \end{bmatrix} \tag{16}$$

In the above equation, $k = \rho a^2$ is the bulk modulus of elasticity of the fluid. Equation (15) can be integrated over an arbitrary finite volume and the volume integral is changed to the surface integral by applying the divergence theorem. After averaging it in the volume, we have

$$\frac{\partial \overline{G}}{\partial t} + \frac{1}{V} \iint_s n \cdot \mathbf{F} \, \mathrm{d}s = 0 \tag{17}$$

where $\overline{G}$ is the volume-averaged value of G, V is the volume, n is the unit normal vector and s is the surface area of the control volume. Equation (15) can be solved by the MacCormack two-step

DOI: 10.1002/fld

explicit predictor–corrector scheme. The time increment is limited by the Courant–Friedrichs–Levy (CFL) condition to meet the numerical stability requirement [18]

$$\Delta t \leqslant \text{Min}\left\{\frac{\text{Volume}}{(|u_i s_i| + a_0|s_i|)}\right\} \tag{18}$$

where u is the velocity and s is the surface area of the control volume.

The maximum allowable time step can be estimated by using the following equation:

$$\Delta t = C_r\left\{\frac{\text{Volume}}{(|u_i s_i| + a_0|s_i|)}\right\} \tag{19}$$

where $0 < C_r < 1$ is the Courant stability factor.

4. NUMERICAL EXPERIMENTATION

The numerical model is applied to a real-world case study of sluice spillway. Spillway consists of seven low-level sluices each of size 8 m wide $\times$12 m height designed to pass the design outflow flood of 10400 m^3/s. The discharge intensity corresponding to a discharge of 10400 m^3/s works out to be 186.43 $m^3/s/m$. In the numerical experimentation, eight different profiles of sluice roof conforming to quarter of an ellipse (see Figure 3) were tested. The length of the sluice bellmouth and location of bellmouth exit are kept the same. Figures 3(a) and (b) are the profiles as per the guidelines of USBR and have zero exit angles and 90° at the bellmouth entry. Figures 3(c) and (d) have 90° entry angle at the bellmouth and exit angles of 3.6 and 5.7°. Figures 3(e)–(h) have acute entry angles and varying exit angles. The discharge of 10400 m^3/s and head over sluice sill of 25.6 m were considered for simulation studies. Each profile was checked for assessing various hydraulic characteristics. Physical model studies were carried out on a 1:45 scale sectional model for the case of sluice spillway with roof profile of Figure 3(a) (profile 1). As a part of validation, the experimental values of pressures, water surface profiles and discharge coefficient obtained from physical model studies were used to compare with the simulated values.

4.1. Mesh system

As the supercritical flow is very sensitive to the geometric boundary conditions, proper representation of the curvilinear spillway profile and free surface is essential to the accurate simulation of the flow over the spillway. For this reason, a boundary-fitted multi-zone structured mesh system is used while developing this model. A boundary-fitted mesh system based on Thompson *et al.*'s method [17] was used to discretize the flow domain. Parts of the prototype simulated in the numerical model include a 42-m long reservoir with water level at 35.6 m and 14-m long sluice barrel and 14.55-m long downstream spillway crest profile conforming to parabolic equation $\mathbf{y} = \mathbf{x}^2/60$. The length of reservoir was selected such that the upstream boundary should be far away from the spillway to avoid the reflection effect. The downstream section has been chosen on a constant sloping section so that zero gradients of velocity and pressure can be assumed. Figure 4 shows the mesh system. The location of the origin of the coordinate system is at the left-hand bottom corner of the mesh system. The computational domain is divided into four zones, discretizing into 12 000 structured quadrilateral cells. Zones 1 and 2 covered the reservoir portion, while zone 3

DOI: 10.1002/fld

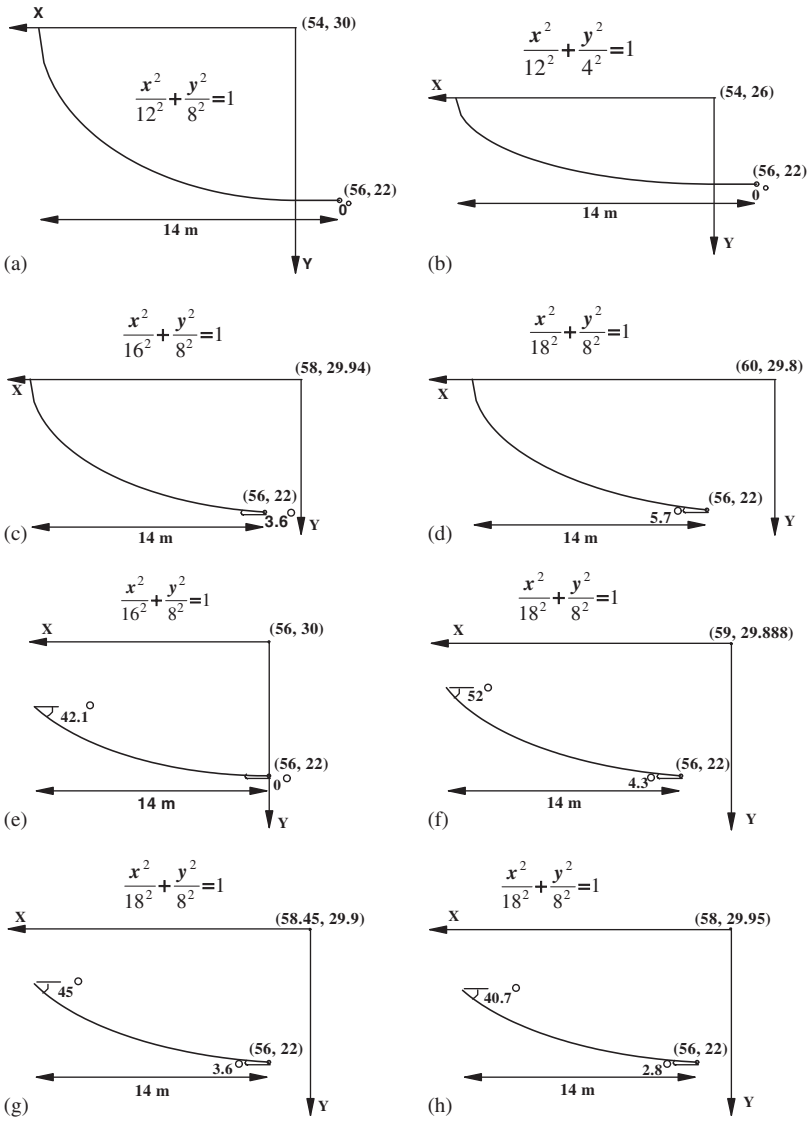

Figure 3. Roof profiles of sluice spillway.

covered the portion of sluice barrel and zone 4 covered the sloping spillway portion downstream of the sluice barrel.

4.2. Boundary and initial conditions

It is intended to simulate the steady-state flow features in the sluice barrel and downstream of sluice spillway when the floodwater is released through the sluice spillway keeping the reservoir

DOI: 10.1002/fld

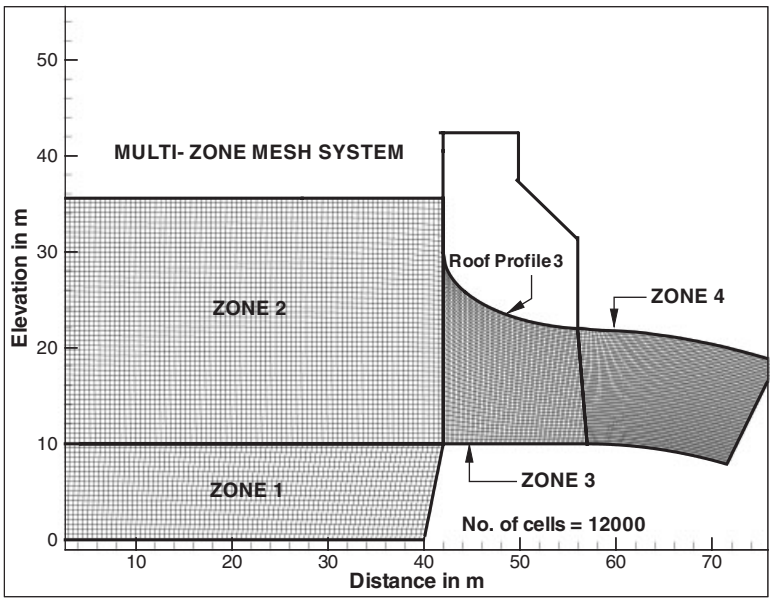

Figure 4. Multi-zone mesh system.

water level constant. In the present study, zones 2 and 4 have free surfaces. Free surface in zone 2 is held constant. The total hydraulic head is the main parameter influencing the flow conditions in the sluice spillway. The contribution of a very small variation in the water surface of the reservoir compared with the total hydraulic head of 25.6 m on the flow field and pressure distribution in the sluice barrel are insignificant. Hence, in the numerical model, a marginal rise in the reservoir water surface is ignored by keeping the reservoir water level constant. Free-surface displacement is allowed in zone 4 by imposing the kinematic and dynamic boundary conditions as described in Section 2.4. According to the kinematic free-surface boundary condition, the fluid particle at each mesh point on the free surface will move to a new location according to the velocity of the particle. New free surface is computed and a new boundary-fitted mesh system is regenerated. The mesh system is updated during the course of simulation until the steady-state solution is reached. Uniform velocity distribution across the depth is used at the upstream open boundary. At the downstream boundary, it is assumed that the flow is fully developed and hence zero-gradient assumption was used for both velocity and pressure. At the solid boundary of the spillway, full slip condition was used for velocity while the centrifugal force is considered when imposing pressure condition.

4.3. Numerical analysis and discussion of results

The main focus of the study was to investigate the effect of geometry of sluice roof profile on the pressure distribution, the discharge coefficient and the nature of flow regime within the sluice bellmouth. Pressures, velocities and other non-dimensional hydraulic parameters such as Froude Number($=V/\sqrt{gd}$) and Cavitation Index ($\sigma=(P_0-P_v)/V_0^2/2g$) were analyzed with respect to

DOI: 10.1002/fld

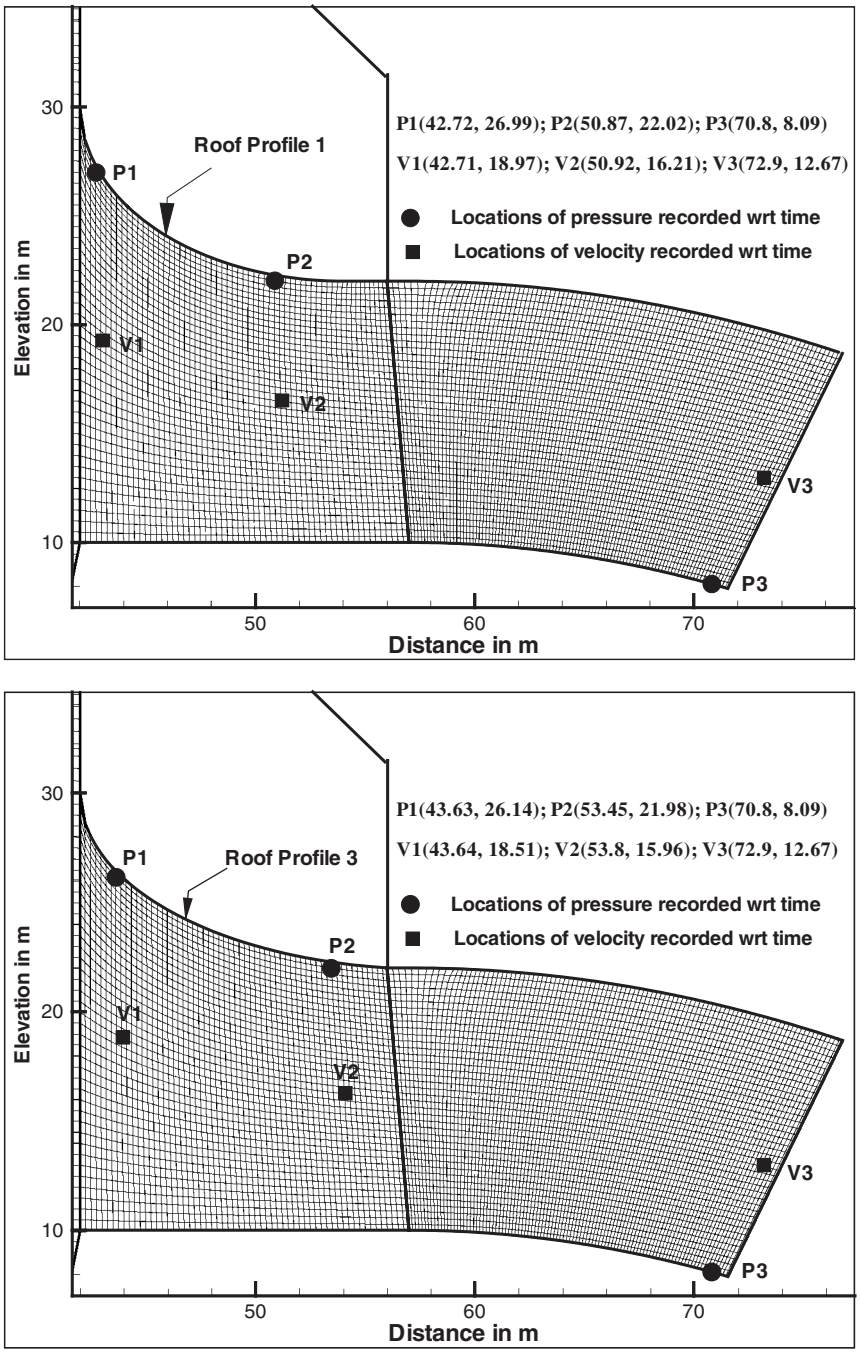

Figure 5. Mesh system showing locations of pressure and velocity recorded for convergence of solution.

DOI: 10.1002/fld

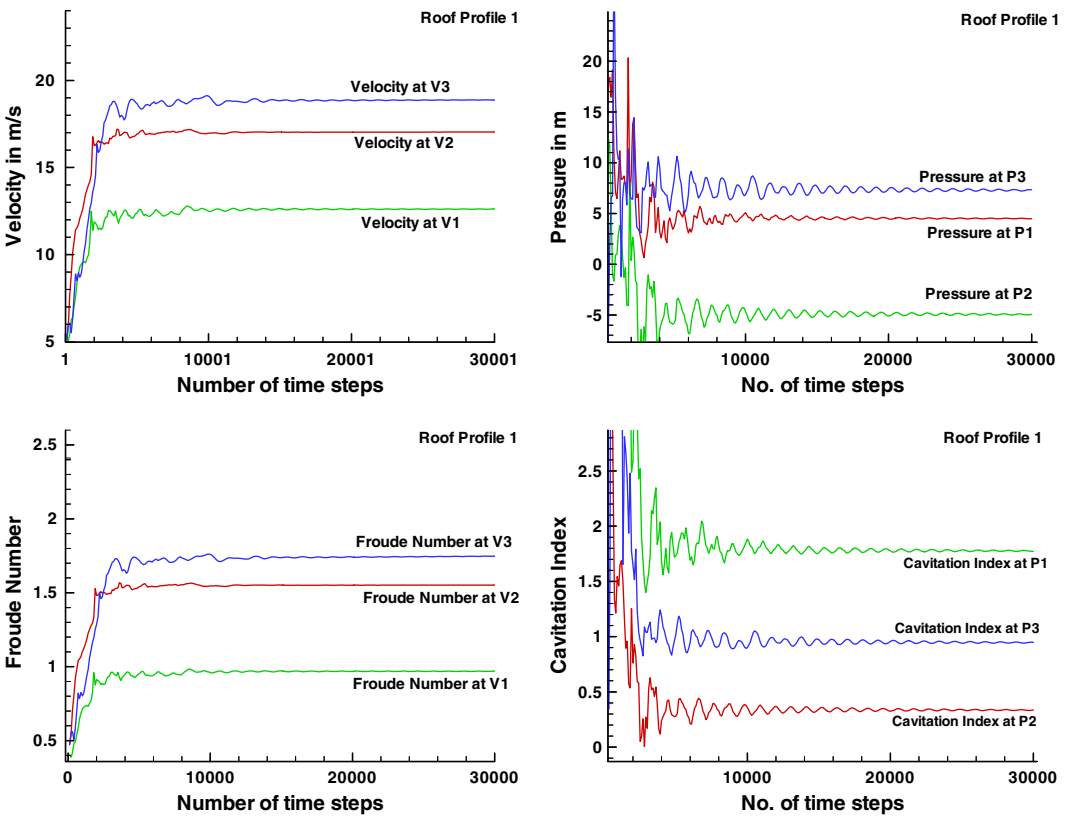

Figure 6. Convergence of various flow parameters at three grid cells (profile 1).

different time steps of simulation. In the above formulae, V is the velocity, d is the depth of water, P_0 is pressure at the point of interest, g is the acceleration due to gravity and P_v is the vapor pressure of fluid. The concept of Froude number applies to a cross section in case of open channel free-surface flow and not for pressurized flow through a closed duct. It is noticed from the physical model studies that the flow through short length sluice barrel do not get fully developed and that flow separation takes place on the sluice roof profile, resulting in negative pressures. The dimension of the sluice barrel in the direction of flow is almost comparable with its height. The state of flow at the entrance of the sluice bellmouth changes from free surface to pressurized flow. The concept of Froude number was applied for locating this critical section where transition condition takes place. This does not have any practical significance. However, it is used to study the occurrence of critical flow (flow transition from subcritical to supercritical) near the entrance of the sluice bellmouth for different roof profiles of sluice spillway in the present case study. While calculating Froude number at a point, the local velocity at a particular grid point and depth of flow at the cross section passing through the grid point are considered.

Three grid locations were selected for pressure and velocity recordings. Figure 5 shows three grid locations each for pressure and velocity recordings. These three locations were selected to cover different types of flows such that the first section lies near the critical flow region, the second

DOI: 10.1002/fld

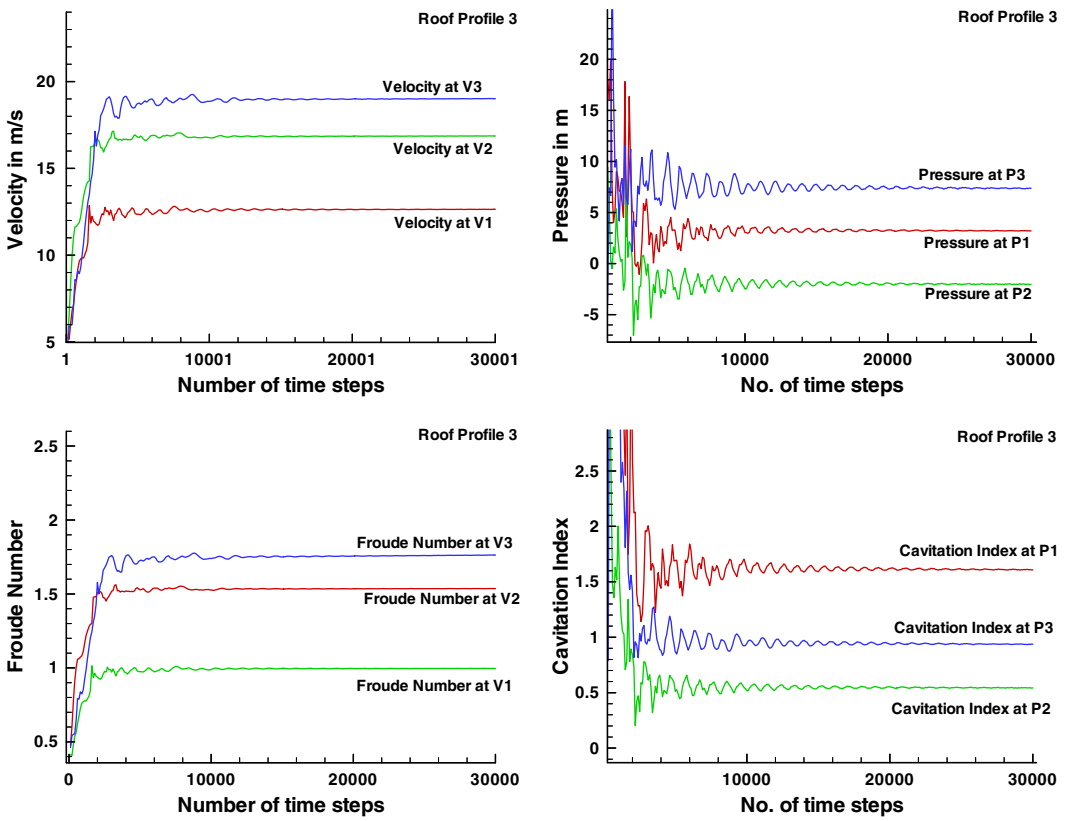

Figure 7. Convergence of various flow parameters at three grid cells (profile 3).

section lies near the minimum pressure zone and the third section at the downstream end of the solution domain. For the sake of brevity and owing to space limitation, the results of only profiles 1 and 3 are included here. Figures 6 and 7 show the convergence of solution for various flow parameters for profiles 1 and 3, respectively. It is noticed that steady-state solution was reached after iterations of 22 000 time steps. As seen from these figures, severe pressure fluctuations were noticed in the beginning but the fluctuations attenuated rapidly reaching steady state around the mean value. Convergence of steady state for velocity parameter was faster than that for the pressure parameter.

The numerical model indicated the occurrence of critical flow at the entrance of the sluice bellmouth at varying distances for different profiles. Flow transition from subcritical to supercritical was noticed at a distance of about 0.5 m downstream from the entry of bellmouth for profiles 1, 2 and 5–8, whereas for profiles 3 and 4 flow transition took place at a distance of 1.7 m. The C_d values, magnitude and location of minimum pressures and location of flow transition from subcritical to supercritical (Froude number = 1) simulated for all the eight profiles were analyzed. Table I shows the details of simulated results. In all cases, cavitation index (σ) works out to be more than 0.2, which is the critical cavitation index recommended by Falvey to avoid cavitation [19]. It has been experienced from physical model studies of various projects that profiles 1 and 2

DOI: 10.1002/fld

Table I. Cavitation index and discharge coefficient for various roof profiles of sluice spillway.

Roof profile no.	Figure no.	Entry angle (deg.)	Exit angle (deg.)	Critical flow location (m)	Minimum pressure on sluice roof			
					Magnitude (m)	Location (m)	σ	C_d
1	3(a)	90	0	42.8	−6.0	(51.56, 22.12)	0.23	0.84
					−5.0*	(51.84, 22.1)*	0.29*	0.79*
2	3(b)	90	0	42.5	−5.4	(49.78, 22.25)	0.26	0.84
3	3(c)	90	3.6	43.7	−2.9	(52.68, 22.37)	0.47	0.83
4	3(d)	90	5.7	43.7	−2.0	(52.56, 22.36)	0.55	0.82
5	3(e)	42.1	0	42.4	−4.2	(51.84, 22.13)	0.38	0.84
6	3(f)	52	4.3	42.7	−2.6	(51.84, 22.37)	0.5	0.83
7	3(g)	45	3.6	42.6	−2.8	(51.96, 22.25)	0.5	0.83
8	3(h)	40.7	2.8	42.5	−3.0	(51.84, 22.37)	0.47	0.83

*The values are from physical model studies.

are susceptible to cavitation damage if spillway is operated with higher heads (say >25 m). Profiles 3–8 with various combination of exit angle and bellmouth entry angle exhibited acceptable pressure distribution with cavitation indices much higher than 0.2. Exit angle is the dominant parameter influencing the pressure distribution on the sluice roof. The cavitation index improved considerably for the profiles with exit angles compared with profiles with zero exit angles. Profiles with exit angles demonstrated gradual improvement in cavitation index with increase in the magnitude of exit angle. The comparative analysis of profiles 1, 2 and 5 (all three profiles are having zero exit angles) showed that profile 5 with entry angle of 42.1° exhibited improved cavitation index compared with 90° entry angle profile.

Profiles with zero degree exit angle tend to give more C_d values due to the presence of large negative pressure zone causing suction but such profiles should be checked for cavitation index. It is quite clear from the present analysis that an exit angle of about 3–4° will improve the cavitation index, yielding acceptable pressure distribution over sluice roof and hence profiles 3 and 6–8 are preferred profiles. Although profile 4 with exit angle more than 5° showed improved pressure distribution, there was reduction in C_d value.

The comparative analysis of discharge characteristics of profiles showed marginal reduction in discharge coefficients (C_d) with exit angle. The cavitation indices of the first two profiles having zero exit angle are very close to 0.2 and hence there is a possibility of inception of cavitation if spillway is operated with higher heads. Comparison of results of the numerical model and the physical model studies conducted for the first profile indicated that the pressure distribution was quite comparable. There was close agreement between the results of the physical and numerical models in simulating the location of low-pressure zone along the roof profile. The computed and experimental values of coefficient of discharge were 0.84 and 0.79. The computed value is higher by 6.3%. The possible reason may be due to the absence of losses due to end contractions because of piers and abutments in the numerical model. For profile 1, the piezometric pressures observed on the physical model were compared with the simulated pressures. Figure 8 shows the pressure distribution in the form of pressure contours (isopressure lines) in the entire flow domain. Figure 9 shows the experimental and simulated pressure distributions on the spillway surface and sluice roof profile. There is a close agreement between the simulated and measured values of roof pressures. Pressures on the bottom surface are not close to those obtained in the physical model. This may

DOI: 10.1002/fld

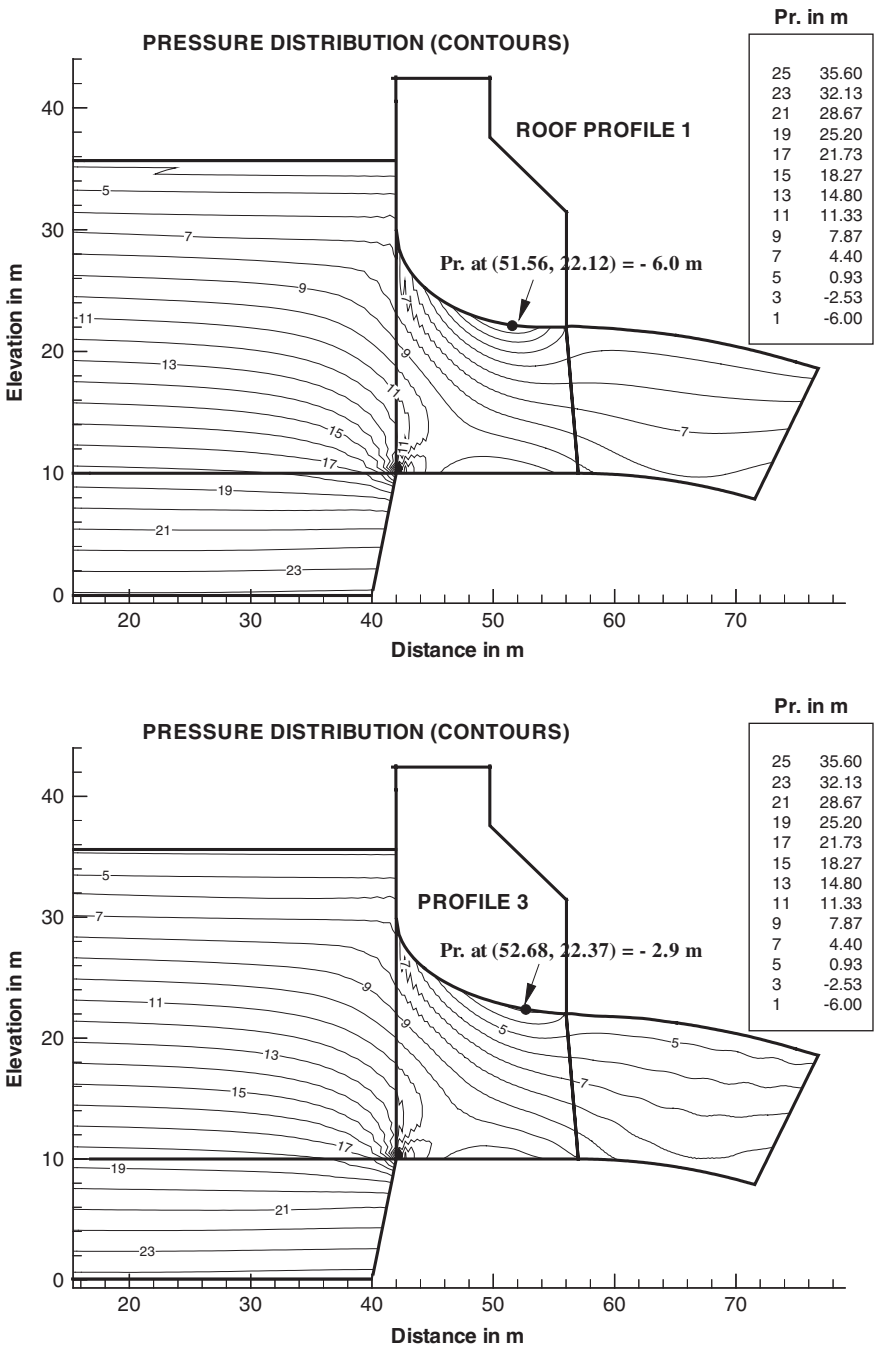

Figure 8. Pressure distribution (in the form of contours).

DOI: 10.1002/fld

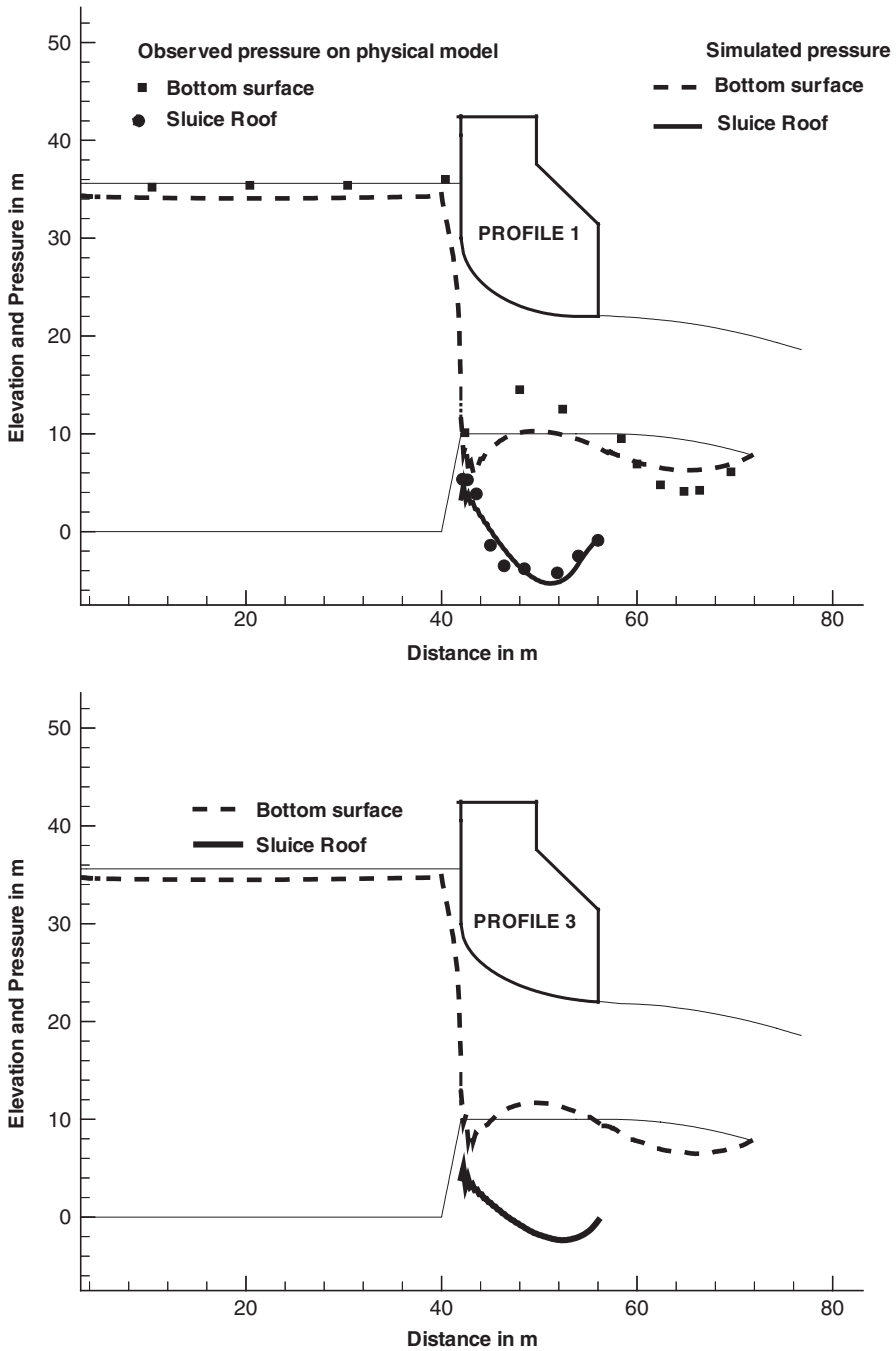

Figure 9. Pressures on spillway and sluice roof profiles.

DOI: 10.1002/fld

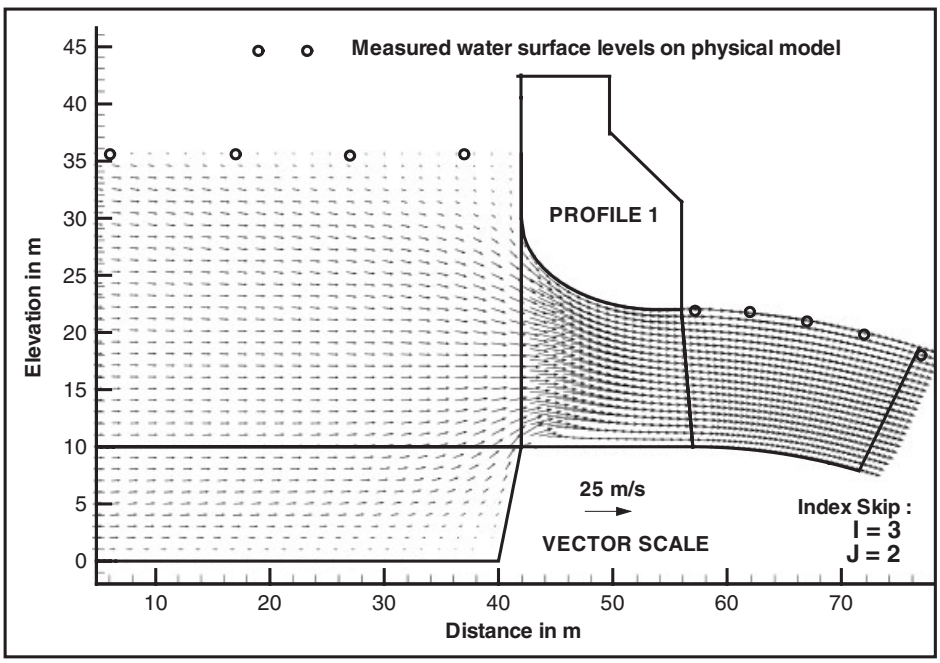

Figure 10. Velocity distribution.

be due to the formation of separation zone on the sill portion owing to the abrupt change in the solid boundary of blunt flat sill portion of sluice spillway and partly due to very high incoming discharge intensity ($186.43\,m^3/s/m$). In reality, this discharge intensity gets reduced considerably due to the wider approach channel upstream of sluice spillway. A separation zone was noticed on the sill level of the sluice at the entrance of the bellmouth as depicted in Figure 10 showing the velocity distribution. The flat bottom sluice profile was not guiding the streamlines entering the sluice from the bottom properly, as a result of which a separation zone was seen on the sill level of the entrance of the sluice (refer Figures 8 and 10).

4.4. Sensitivity analysis

The developed numerical algorithm is based on the explicit scheme. The requirement of computational time step is dictated by the CFL condition for numerical stability. Also, weakly compressible flow equations are low Mach number flows. The range of Mach number needs to be calibrated. In the present numerical simulation, sound speed in water is assumed in the non-dimensional form of Mach number (ratio of speed of flow to speed of sound). Mach number of 0.02 and Courant number (Courant stability factor) of 0.8 are used in the numerical simulation. Sluice spillway with roof profile 1 was employed to perform the sensitivity analysis for the parameters of Mach number and Courant number to investigate their influence on the numerical solution. Sensitivity analysis was done for 24 different combinations of six Mach numbers (0.01, 0.02, 0.03, 0.04, 0.05 and 0.1) and four Courant numbers (0.6, 0.7, 0.8 and 0.9). Table II summarizes the mutual influence of Mach number and Courant number on the convergence of the solution. It may be seen from the

DOI: 10.1002/fld

Table II. Sensitivity analysis of Mach number and Courant number—number of time steps for convergence of solution (coarse mesh system; no. of cells = 12 000).

	Mach no.					
Courant no.	0.01	0.02	0.03	0.04	0.05	0.1
0.6	53 000	27 000	13 700	12 000	11 700	11 500
0.7	46 000	24 400	11 700	11 400	11 000	10 600
0.8	45 000	22 000	10 300	10 800	10 500	Diverges
0.9	42 000	17 000	10 100	8500	8000	Diverges

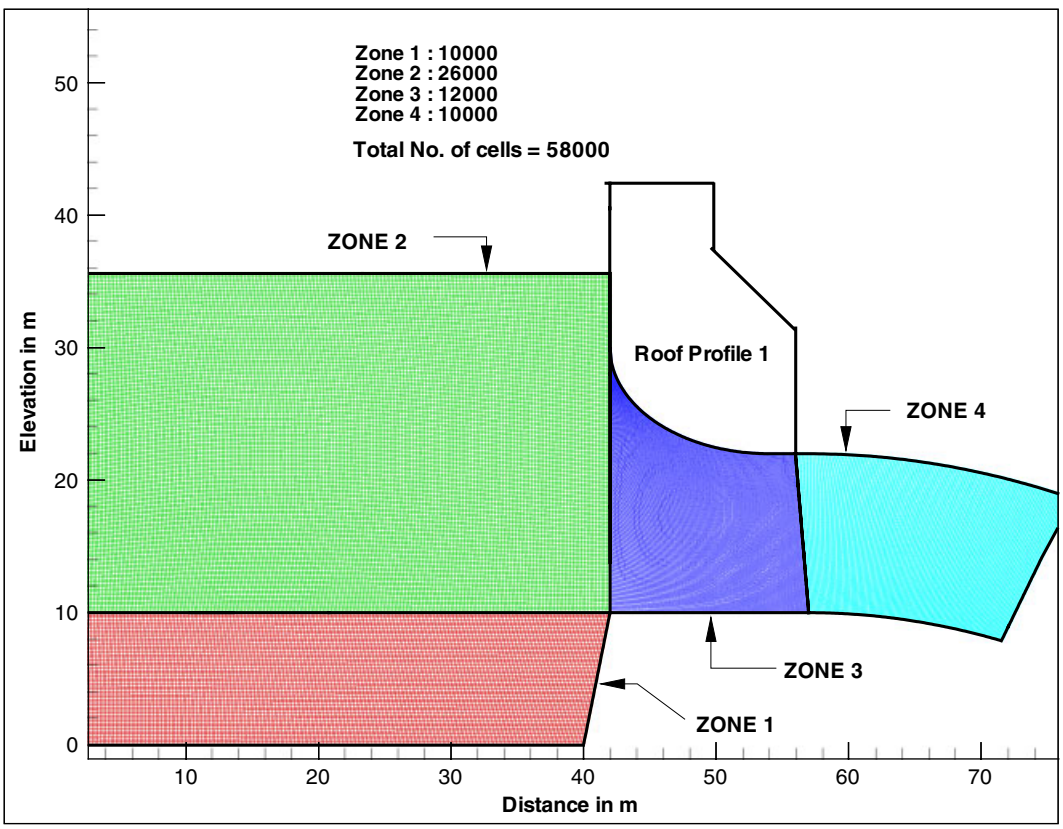

Figure 11. Multi-zone fine mesh system.

table that convergence was faster for higher values of Courant number and Mach number. However, for the combination of Courant number = 0.9 and Mach number = 0.1 and for higher values, the solution was diverging with strong numerical oscillations. The same solution was obtained for any given combination within certain range of Courant numbers and Mach numbers. According to the authors' experiences while simulating hydrodynamics of spillway flows, Mach number of 0.02 and Courant number of 0.8 gave satisfactory results.

DOI: 10.1002/fld

Table III. Sensitivity analysis of Mach number and Courant number—number of time steps for convergence of solution (fine mesh system; no. of cells = 58 000).

	Mach no.				
Courant no.	0.01	0.02	0.03	0.04	0.05
0.6	104 000	74 000	44 300	36 600	27 200
0.7	93 000	63 500	38 200	32 800	25 600
0.8	84 000	53 000	32 800	28 900	22 500
0.9	77 500	50 400	30 800	25 600	19 700

Table IV. Comparison of various hydraulic parameters simulated at three grid locations.

Hydraulic parameter	Grid location in m	Fine mesh system	Coarse mesh system	% Difference
Velocity in m/s	V_1 (43.3, 16.7)	13.22	13.37	1.1
	V_2 (50.89, 16.2)	17.06	17.06	0.0
	V_3 (73.12, 13.64)	18.7	18.7	0.0
Pressure in m	P_1 (43.3, 26.55)	2.8	2.7	−0.8
	P_2 (51.1, 22.03)	−5.47	−5.46	0.2
	P_3 (70.7, 8.13)	7.5	7.47	−0.2
Froude number	V_1 (43.3, 16.7)	1.04	1.05	1.0
	V_2 (50.89, 16.2)	1.56	1.57	0.6
	V_3 (73.12, 13.64)	1.72	1.73	0.6
Cavitation index	P_1 (43.3, 26.55)	1.4	1.38	−1.4
	P_2 (51.1, 22.03)	0.3	0.299	−0.3
	P_3 (70.7, 8.13)	0.98	0.97	−1.0

A research study such as the one described in this paper must include grid convergence as part of the numerical modeling efforts. The grid appears too coarse in the reservoir portion. The flow in the reservoir does not show much variation within the coarse grid owing to tranquil nature of flow in the reservoir portion. Our experience with other case studies has indicated that solution was independent of grid resolution for such mesh sizes in the reservoir portion. One does not know how fine a grid must be used without conducting a grid convergence. Grid convergence requires that the grid be refined until the solution becomes indifferent to finer resolution. The possibility of discretization error was checked to find out whether or not the solution is grid independent by carrying out simulation studies with fine mesh system (no. of cells = 58 000) for roof profile 1. Figure 11 shows the fine mesh system used. Sensitivity analysis was done for 20 different combinations of five Mach numbers (0.01, 0.02, 0.03, 0.04 and 0.05) and four Courant numbers (0.6, 0.7, 0.8 and 0.9). When grid size was refined, requirement of time steps was more. Table III summarizes the mutual influence of Mach number and Courant number on the number of time steps required for convergence of the solution. The comparison of simulated values of various hydraulic parameters at three grid locations using coarse mesh system and fine mesh system indicated the close agreement between each other as the difference between the values was less than 1%. Table IV gives the comparison of simulated values of various hydraulic parameters at three grid locations using coarse and fine mesh systems. Simulation with fine mesh system indicated that the computed value of coefficient of discharge was 0.83, which is higher by 5% compared with the experimental value of 0.79.

DOI: 10.1002/fld

5. CONCLUSIONS

In this paper, Euler-based 2-D weakly compressible flow model is applied to simulate flow through sluice spillway. Following are some useful guidelines that can be drawn from the analysis of results, which are of practical relevance to design engineers.

- Profiles with exit angles demonstrated gradual improvement in cavitation index with increase in the magnitude of exit angle. It is recommended to provide an exit angle of about 3–4° to have acceptable pressure distribution yielding higher cavitation index.
- Profiles with 90° entry angle and 0° exit angle yield more C_d values due to the presence of large negative pressure zone causing suction, but these profiles are susceptible to cavitation damage when operated with high heads.
- The computed values of coefficient of discharge are higher by 6 and 5% for coarse and fine mesh systems, respectively, when compared with the experimental value.
- Sensitivity analysis of Mach number and Courant number on the numerical solution indicated that the convergence was faster for higher values of Courant number and Mach number. However, beyond a certain range of values, the solution was diverging with strong numerical oscillations.
- The possibility of discretization error was checked to find out whether or not the solution is grid independent by carrying out simulation studies with coarse and fine mesh systems. The close agreement (less than 1%) between each other indicated that the solution is independent of the grid size chosen.

ACKNOWLEDGEMENTS

The authors are grateful to Prof. Charles C. S. Song, University of Minnesota, U.S.A. and Director, Central Water and Power Research Station, Pune, India, for encouraging to pursue the studies and providing facilities and training on model development described in this paper.

REFERENCES

1. United States Bureau of Reclamation (USBR). *Design of Small Dams* (3rd edn). US Govt. Printing Office: Washington, DC, 1987.
2. Li W, Xie Q, Chen CJ. Finite analytical solution of flow over spillway. *Journal of Engineering Mechanics* (ASCE) 1989; **115**(12):2635–2647.
3. Olsen NR, Kjellesvig HM. 3-D Numerical flow modeling for estimation of spillway capacity. *Journal of Hydraulic Research* (IAHR) 1998; **36**(5):775–784.
4. Burgisser MF, Rutschmann P. Numerical solution of viscous 2DV free surface flows: flow over spillway crests. *Proceedings of the 28th IAHR Congress*, Technical University, Graz, Austria, 1999.
5. Chen Q, Dai G, Liu H. Volume of fluid model for turbulence numerical simulation of stepped spillway overflow. *Journal of Hydraulic Engineering* (ASCE) 2002; **128**(7):683–688.
6. Wenli W, Huichao D. Simulation of turbulence flows on concave surfaces of spillways including the effects of streamline curvature. *Proceedings of the XXXI IAHR Congress*, Seoul, Korea, 2005; 2589–2597.
7. Yang J, Johansson N. Determination of spillway discharge capacity—CFD modeling and experiment verification. *Proceedings of 3rd International Conference on Hydro-Science and Engineering*, Berlin, Germany, 1998.
8. Savage BM, Johnson MC. Flow over ogee spillway; physical and numerical model case study. *Journal of Hydraulic Engineering* (ASCE) 2001; **127**(8):640–649.
9. Jean C, Mazen T. Computational modeling of flow over an ogee spillway. *Journal of Computers and Structures* 2004; **82**:1805–1812.

DOI: 10.1002/fld

10. Unami K, Kawachi T, Munir Baber M, Itagaki H. Two-dimensional numerical model of spillway flow. *Journal of Hydraulic Engineering* (ASCE) 1999; **125**(4):369–375.
11. Zhou F, Bhajantri MR. Numerical study of the effects of spillway crest shape on the distribution of pressure and discharge. *Proceedings of the 3rd International Conference on Hydro-Science and Engineering*, Berlin, Germany, 1998.
12. Song CCS, Zhou F. Simulation of free surface flow over spillway. *Journal of Hydraulic Engineering* (ASCE) 1999; **125**(9):959–967.
13. Song CCS, Yuan MA. Weakly compressible flow model and rapid convergence methods. *Journal of Fluid Engineering* (ASME) 1988; **110**:441–445.
14. Bhajantri MR, Eldho TI, Deolalikar PB. Modeling hydrodynamic flow over spillway using weakly compressible flow equations. *Journal of Hydraulic Research* (IAHR) 2007; P2905.
15. Bhajantri MR, Eldho TI, Deolalikar PB. Numerical modeling of turbulent flow through sluice spillway with gated operation. *International Journal for Numerical Methods in Engineering* 2007; **72**:221–243.
16. MacCormack RW. Effect of viscosity in hypervelocity impact cratering. *American Institute of Aeronautics and Astronautics* (AIAA) 1969; **7**:69–354.
17. Thompson JF, Warsi ZUA, Martin CW. *Numerical Grid Generation—Foundations and Applications*. North-Holland: Amsterdam, 1985.
18. Courant R, Friedrichs KO, Lewy H. On the partial differential equations of mathematical physics. *IBM Journal of Research Development* 1967; **11**:215–234.
19. Falvey HT. Cavitation in chutes and spillways. *USBR Engineering Monograph No. 42*, A Water Resources Technical Publication: Denver, CO, 1990.

DOI: 10.1002/fld